

~~CONFIDENTIAL~~

UNCLASSIFIED

NACA RM L55F21



# RESEARCH MEMORANDUM

WIND-TUNNEL INVESTIGATION AT LOW SPEED  
OF SIDESLIPPING, ROLLING, YAWING, AND PITCHING  
CHARACTERISTICS FOR A MODEL OF A 45° SWEEP-WING  
FIGHTER-TYPE AIRPLANE FOR REFERENCE

By Byron M. Jaquet and H. S. Fletcher

Langley Aeronautical Laboratory NOT TO BE TAKEN FROM THIS ROOM  
Langley Field, Va.

CLASSIFICATION CHANGED

UNCLASSIFIED

To \_\_\_\_\_

By authority of TPA # 39 Date 1/12/61 CLASSIFIED DOCUMENT

This material contains information affecting the National Defense of the United States within the meaning of the espionage laws, Title 18, U.S.C., Secs. 793 and 794, the transmission or revelation of which in any manner to an unauthorized person is prohibited by law.

## NATIONAL ADVISORY COMMITTEE FOR AERONAUTICS

WASHINGTON

September 1, 1955

~~CONFIDENTIAL~~

UNCLASSIFIED



## NATIONAL ADVISORY COMMITTEE FOR AERONAUTICS

## RESEARCH MEMORANDUM

WIND-TUNNEL INVESTIGATION AT LOW SPEED  
OF SIDESLIPPING, ROLLING, YAWING, AND PITCHING  
CHARACTERISTICS FOR A MODEL OF A 45° SWEPT-WING  
FIGHTER-TYPE AIRPLANE

By Byron M. Jaquet and H. S. Fletcher

## SUMMARY

An investigation was made in the Langley stability tunnel at low speed to determine the rolling characteristics (ailerons undeflected and deflected) at combined angles of attack and sideslip for an 0.0825-scale model of a fighter-type airplane having a 45° sweptback wing. The tests were made with the original vertical tail and with a vertical tail that had an exposed area which was about 27 percent larger. In addition, the static longitudinal and lateral characteristics were determined. The yawing derivatives were obtained at various angles of attack and sideslip, and the pitching derivatives were obtained for various angles of attack and zero angle of sideslip. The directional stability and damping in yaw of the airplane corresponding to the model of the present investigation and of several other high-speed airplanes were compared on the basis of wing, vertical-tail, or fuselage dimensions.

In order to expedite publication, no extensive analysis of the data has been made.

## INTRODUCTION

During recent flight tests of a swept-wing fighter airplane (ref. 1), extremely violent, uncontrolled longitudinal and lateral motions occurred at a Mach number of about 0.7 and an altitude of about 30,000 feet in rudder-fixed left aileron rolls. In these rolls, initiated by the application of two-thirds or more of the total aileron deflection, very large negative angles of attack and left sideslip were attained which resulted in high load factors.

In the Langley stability tunnel it is possible to obtain the rolling and yawing derivatives of models at combined angles of attack and sideslip. Thus, in order to provide information relative to the uncontrolled motions of the fighter airplane of reference 1, an investigation was made of an 0.0825-scale model of the airplane with the original vertical tail and with a vertical tail that had an exposed area which was about 27 percent larger. The purpose of this investigation was to determine the rolling derivatives and the effect of aileron deflection on these derivatives for various angles of attack and sideslip. In addition, the static longitudinal and lateral characteristics (ailerons undeflected and deflected) were determined. The yawing derivatives were also determined with the ailerons undeflected and deflected for various angles of attack and sideslip. The pitching derivatives were obtained at various angles of attack at zero angle of sideslip with the ailerons undeflected and deflected.

In order to expedite publication, no extensive analysis of the data has been made.

#### SYMBOLS

The data presented herein are referred to the stability system of axes (except as noted). The origin of the axes system was at the center of gravity of the model, which was coincident with the 0.32 mean aerodynamic chord of the wing. The positive directions of the forces, moments, and angular displacements are shown in figure 1. The symbols and coefficients are defined as follows:

L	lift, lb
D	drag, lb
Y	lateral force, lb
M	pitching moment, ft-lb
L'	rolling moment, ft-lb
N	yawing moment, $N = N_w$ , ft-lb
A	aspect ratio (refers to wing unless otherwise indicated by subscript), $b^2/S$
b	span (refers to wing unless otherwise indicated by subscript), ft

- S area (refers to wing unless otherwise indicated by subscript), sq ft
- $D_F$  maximum fuselage depth, excluding canopy, ft
- $l_F$  fuselage length, excluding booms, ft
- $l$  tail length, measured parallel to fuselage reference line from center of gravity to  $\bar{c}/4$  of tail, ft
- $c$  chord measured parallel to plane of symmetry (refers to wing unless otherwise indicated by subscript), ft
- $\bar{c}$  mean aerodynamic chord (refers to wing unless otherwise indicated by subscript),  $\frac{2}{S} \int_0^{b/2} c^2 dy$ , ft
- $y$  spanwise distance measured from and perpendicular to plane of symmetry (refers to wing unless otherwise indicated by subscript), ft
- $\alpha$  angle of attack of fuselage reference line, deg
- $\beta$  angle of sideslip, deg
- $\psi$  angle of yaw, radians
- $\gamma$  angle of climb, radians
- $\theta$  angle of pitch, radians
- $\phi$  angle of bank, radians
- $\delta_{aL}$  angle of deflection of left aileron, measured perpendicular to hinge line, deg
- $\delta_{aR}$  angle of deflection of right aileron, measured perpendicular to hinge line, deg
- $q_0$  free-stream dynamic pressure,  $\rho v^2/2$ , lb/sq ft
- $\rho$  mass density of air, slugs/cu ft
- $v$  free-stream velocity, ft/sec

- $p$  rolling angular velocity for stability-axes system,  
 $p = p_w \cos \beta - q_w \sin \beta$  or  $\frac{d\phi}{dt}$ , radians/sec
- $p_w$  rolling angular velocity measured about wind X-axis, radians/sec
- $q$  pitching angular velocity for stability-axes system,  
 $q = q_w \cos \beta + p_w \sin \beta$  or  $\frac{d\theta}{dt}$ , radians/sec
- $q_w$  pitching angular velocity about wind Y-axis (for the present investigation,  $q = q_w$  since  $\beta = 0^\circ$ ), radians/sec
- $r$  yawing angular velocity about vertical axis,  $\frac{d\psi}{dt}$ , radians/sec
- $t$  time, sec
- $\frac{p_w b}{2V}$  rolling-angular-velocity parameter, radians
- $\frac{q \bar{c}}{2V}$  pitching-angular-velocity parameter, radians
- $\frac{r b}{2V}$  yawing-angular-velocity parameter, radians
- $C_L$  lift coefficient,  $L/q_0 S$
- $C_D$  drag coefficient,  $D/q_0 S$
- $C_Y$  lateral-force coefficient,  $Y/q_0 S$
- $C_l$  rolling-moment coefficient,  $L'/q_0 S b$
- $C_n$  yawing-moment coefficient,  $N/q_0 S b$
- $C_m$  pitching-moment coefficient,  $M/q_0 S \bar{c}$
- $C_{Y\beta} = \frac{\partial C_Y}{\partial \beta}$
- $C_{n\beta} = \frac{\partial C_n}{\partial \beta}$

$$C_{L\beta} = \frac{\partial C_L}{\partial \beta}$$

$$\left. (\Delta C_{Y\beta})_{p_w} \right\}$$

$$\left. (\Delta C_{n\beta})_{p_w} \right\}$$

$$\left. (\Delta C_{L\beta})_{p_w} \right\}$$

Increments in derivatives due to  $\frac{p_w b}{2V}$

$$C_{Yr} = \frac{\partial C_Y}{\partial \left(\frac{rb}{2V}\right)}$$

$$C_{nr} = \frac{\partial C_n}{\partial \left(\frac{rb}{2V}\right)}$$

$$C_{Lr} = \frac{\partial C_L}{\partial \left(\frac{rb}{2V}\right)}$$

$$C_{Yp} = \frac{\partial C_Y}{\partial \left(\frac{p_w b}{2V}\right)}$$

$$C_{np} = \frac{\partial C_n}{\partial \left(\frac{p_w b}{2V}\right)}$$

$$C_{Lp} = \frac{\partial C_L}{\partial \left(\frac{p_w b}{2V}\right)}$$

$$C_{Lq} = \frac{\partial C_L}{\partial \left(\frac{q\bar{c}}{2V}\right)}$$

$$C_{Dq} = \frac{\partial C_D}{\partial \left(\frac{q\bar{c}}{2V}\right)}$$

$$C_{mq} = \frac{\partial C_m}{\partial \left( \frac{q\bar{c}}{2V} \right)}$$

Subscripts:

w referred to wind system of axes

$V_e$  exposed vertical tail

h horizontal tail

#### APPARATUS AND MODEL

The tests of the present investigation were made in the 6-foot-diameter rolling-flow test section (ref. 2) and in the 6- by 6-foot curved-flow test section (ref. 3) in the Langley stability tunnel. In these test sections, rolling, yawing, or pitching flight is simulated by rolling or curving the airstream about a stationary model mounted on a support strut.

A drawing of the model used in this investigation is presented as figure 2, and additional information is given in table I. Drawings of model 2 of reference 4 were obtained and the dimensions were reduced to a size suitable for the Langley stability tunnel. Two different fuselage-nose lengths were investigated.

The wing was constructed of laminated mahogany with a dural trailing edge to prevent warping. A 1/4-inch-thick dural plate extended 4 inches to either side of the plane of symmetry to insure adequate stiffness of the wing.

The small vertical tail and the horizontal tail were constructed of laminated mahogany with a 1/8-inch-thick dural core for stiffness. A vertical tail that had an area which was about 27 percent larger than the original tail was constructed of solid spruce with a modified  $3\frac{1}{2}$ -percent-thick flat-plate airfoil section. The quarter-chord line of this larger vertical tail was coincident with that of the small vertical tail.

#### TESTS

Several types of tests were made at a dynamic pressure of 24.9 lb/sq ft, a Mach number of 0.13, and a Reynolds number of  $0.88 \times 10^6$ .

The static longitudinal characteristics were determined at  $\beta = 0^\circ$  for an angle-of-attack range from  $-30^\circ$  to  $30^\circ$ , and the static lateral derivatives were determined at  $\beta = \pm 3^\circ$  for an angle-of-attack range from  $-30^\circ$  to  $30^\circ$ . A few tests were made through a sideslip-angle range from  $3^\circ$  to  $-12^\circ$  for angles of attack of  $0^\circ$ ,  $-3^\circ$ ,  $-6^\circ$ , and  $-12^\circ$ .

The rolling derivatives were determined over an angle-of-attack range from  $-12^\circ$  to  $12^\circ$  for values of  $\frac{p_w b}{2V} = -0.0708, -0.0462, -0.0269, 0.0072, 0.0313,$  and  $0.0613$  at sideslip angles of  $0^\circ, -3^\circ, -6^\circ,$  and  $-12^\circ$ .

In order to determine the effect of  $\frac{p_w b}{2V}$  on the static lateral derivatives, tests were made at  $\beta = \pm 6^\circ$  at values of  $\frac{p_w b}{2V} = -0.0708, 0,$  and  $0.0613$  for the small vertical-tail configuration only.

The yawing derivatives were determined for an angle-of-attack range from  $-12^\circ$  to  $12^\circ$  for sideslip angles of  $0^\circ, -3^\circ, -6^\circ,$  and  $-12^\circ$  at values of  $\frac{r_b}{2V} = 0, -0.0314, -0.0665,$  and  $-0.0875$ . The pitching derivatives were determined for an angle-of-attack range from  $-12^\circ$  to  $12^\circ$  for  $\beta = 0^\circ$  only and at values of  $\frac{q_c}{2V} = 0, 0.0097, 0.0206,$  and  $0.0271$ .

The tests were made with the ailerons undeflected and with the left-aileron trailing edge up  $20^\circ$  and the right-aileron trailing edge down  $20^\circ$ . The tests were repeated for the model with the large vertical tail except that the rolling and yawing derivatives were only determined at  $\beta = 0^\circ$  and  $-6^\circ$ .

#### CORRECTIONS

The angle of attack and the drag coefficient have been corrected for the effects of the jet boundaries by the methods of reference 5. The pitching-moment coefficient for horizontal-tail-on configurations were corrected by the methods of reference 6. The data have not been corrected for the effects of blockage or support-strut tares. The yawing and pitching derivatives have been corrected for the cross-tunnel pressure gradient that exists in curved flow.

The rolling derivatives  $C_{l_p}, C_{n_p},$  and  $C_{y_p}$  which are given for angles of sideslip other than zero have not been corrected for the effective pitching velocity induced by virtue of the airstream being rolled

about the wind axes in sideslip. At an angle of attack of  $-12^\circ$  and an angle of sideslip of  $-12^\circ$  (where the value of  $C_{l_p}$  is smallest), the correction to  $C_{l_p}$  would amount to about 9 percent, the corrected value of  $C_{l_p}$  being more negative and the effect of sideslip being reduced. The correction to  $C_{n_p}$  amounts to a maximum of 3 percent at a sideslip angle of  $-12^\circ$ , and the correction to  $C_{Y_p}$  is negligible for all conditions. If it is desired to apply these corrections to  $C_{l_p}$  and  $C_{n_p}$  for angles of sideslip other than zero, the following equations should be used:

$$(C_{l_p})_{\text{corrected}} = C_{l_p} \cos \beta + C_{m_q} \left(\frac{\bar{c}}{b}\right)^2 \sin^2 \beta$$

$$(C_{n_p})_{\text{corrected}} = C_{n_p} \cos \beta$$

Where  $C_{l_p}$  and  $C_{n_p}$  are the values given in figures 8 and 9 for the corresponding value of  $\beta$  in question and  $C_{m_q}$  is obtained from figure 12. It was not possible to obtain  $C_{m_q}$  at sideslip angles other than zero and, hence, in applying the correction to  $C_{l_p}$ , it must be assumed that  $C_{m_q}$  does not vary with angle of sideslip, which may or may not be the case. At zero angle of sideslip there are no corrections, of course.

## RESULTS

### Presentation of Data

The variation of  $C_m$ ,  $C_L$ , and  $C_D$  with  $\alpha$  at  $\beta = 0^\circ$  is presented in figure 3 for several arrangements of the model. In figure 4 the variation of the derivatives  $C_{Y_\beta}$ ,  $C_{n_\beta}$ , and  $C_{l_\beta}$  with  $\alpha$  is presented for the model (with ailerons undeflected and deflected) with the small

and large vertical tail, and the effect of  $p_w b/2V$  on the variation of  $(\Delta C_{Y\beta})_{P_w}$ ,  $(\Delta C_{n\beta})_{P_w}$ , and  $(\Delta C_{l\beta})_{P_w}$  with  $\alpha$  for the model with the small vertical tail is presented in figure 5. In figures 6 and 7 the variation of  $C_Y$ ,  $C_m$ ,  $C_n$ , and  $C_l$  with  $\beta$  and  $\alpha$  is shown for the model with the small and large vertical tails (ailerons deflected and undeflected), respectively.

In figures 8 and 9 the variation of  $C_{Y_p}$ ,  $C_{n_p}$ , and  $C_{l_p}$  with  $\alpha$  and  $\beta$  is presented for the model with the small and large vertical tail, respectively. The derivatives  $C_{l_p}$  and  $C_{n_p}$  may be corrected for the effects of induced pitching velocity as indicated in the section entitled "Corrections." The variation of the yawing derivatives  $C_{Y_r}$ ,  $C_{l_r}$ , and  $C_{n_r}$  with  $\alpha$  and  $\beta$  is presented in figures 10 and 11 for the model with the small and large vertical tail, respectively. The variation of the pitching derivatives  $C_{L_q}$ ,  $C_{D_q}$ , and  $C_{m_q}$  with  $\alpha$  (at  $\beta = 0^\circ$  only) for the model with either the small or the large vertical tail is presented in figure 12.

#### General Remarks

In order to expedite publication of the results of this investigation, no extensive analysis has been made; however, there are a few results that may be of particular significance with respect to the uncontrolled motions of the fighter airplane mentioned in reference 1. These points are mentioned herein in order that they will not be overlooked in an examination of the figures.

A region of about neutral static longitudinal stability existed at negative angles of attack from about  $-9^\circ$  to  $-20^\circ$ , which was slightly greater than the region of neutral stability that existed at positive angles of attack from  $9^\circ$  to  $13^\circ$  (fig. 3). The directional stability (fig. 4) of the model with the small vertical tail decreased with an increase in angle of attack until at about  $\alpha = 15^\circ$ ,  $C_{n\beta}$  became zero. With the large vertical tail,  $C_{n\beta} = 0$  was not obtained until  $\alpha = 25^\circ$  was reached. The sideslip derivatives were relatively unaffected by aileron deflection and rolling velocity (figs. 4 to 7). Appreciable variations occurred in the pitching moment with sideslip when the ailerons were deflected although little change occurred when the ailerons were undeflected (figs. 6 and 7). The rolling derivatives were not greatly affected by aileron deflection or sideslip angle although an appreciable

positive shift in  $C_{n_p}$  occurred at negative angles of attack as the sideslip angle was changed from  $0^\circ$  to  $-11.8^\circ$  (fig. 8). The most apparent effect of sideslip on the yawing derivatives was an increase of about 40 percent in  $C_{n_r}$  at zero angle of attack which decreased with either a positive or negative change in angle of attack (fig. 10). Aileron deflection appeared to be of secondary importance with regard to the yawing derivatives. When the ailerons were deflected (fig. 12) there was less of an increase in the damping in pitch  $C_{m_q}$  at positive angles of attack.

The derivatives  $C_{n_\beta}$  and  $C_{n_r}$  are of primary importance with respect to the directional stability and lateral damping of airplanes. For the present airplane and several other high-speed airplanes (see drawings in fig. 13), these derivatives are compared on three different bases in figure 14. In the upper part of the figure the derivatives are plotted against angle of attack. The middle part of the figure presents the derivatives nondimensionalized to show the amount of directional stability and damping in yaw per unit of tail effectiveness. The units of tail effectiveness are considered to be  $S_{V_e} l_e$  for  $C_{n_\beta}$  and  $S_{V_e} l_e^2$  for  $C_{n_r}$ , inasmuch as the contribution of the vertical tail to these derivatives is proportional to these factors. The factor  $C_{n_\beta} (S_b / S_{V_e} l_{V_e})$  is essentially the lift-curve slope of the vertical tail with all interference and sidewash effects included. The lower part of the figure gives the directional stability and damping in yaw nondimensionalized to show the directional stability and damping in yaw per unit of fuselage directional instability. The units of fuselage directional instability are considered to be  $D_F^2 l_F$ , inasmuch as the contribution of the fuselage to the directional-stability derivative is proportional to this factor. The derivatives of the airplanes, other than that of the present investigation, were obtained from reference 7 and unpublished data.

An examination of figure 14 shows that, on all bases considered, the directional stability of the airplane with the small vertical tail is low compared to the rest of the airplanes and the directional stability of airplane A is large.

The damping in yaw of all airplanes, except airplane A, is about the same at low angles of attack when it is nondimensionalized relative to the fuselage size. The damping in yaw per unit of tail effectiveness (middle part of fig. 14) varied widely for the different airplanes, which indicates a considerable difference in the efficiency of the vertical tail

area employed in producing damping in yaw. The effectiveness of the vertical tail in producing damping in yaw is affected by many things; a few are: wing position, the canopy, fuselage-wing interference, and vertical-tail size. High-aspect-ratio tails and tails near large fuselages are very effective in producing damping in yaw.

Langley Aeronautical Laboratory,  
National Advisory Committee for Aeronautics,  
Langley Field, Va., June 14, 1955.

## REFERENCES

1. NACA High-Speed Flight Station: Flight Experience With Two High-Speed Airplanes Having Violent Lateral-Longitudinal Coupling in Aileron Rolls. NACA RM H55A13, 1955.
2. MacLachlan, Robert, and Letko, William: Correlation of Two Experimental Methods of Determining the Rolling Characteristics of Unswept Wings. NACA TN 1309, 1947.
3. Bird, John D., Jaquet, Byron M., and Cowan, John W.: Effect of Fuselage and Tail Surfaces on Low-Speed Yawing Characteristics of a Swept-Wing Model As Determined in Curved-Flow Test Section of the Langley Stability Tunnel. NACA TN 2483, 1951. (Supersedes NACA RM L8G13.)
4. Blanchard, Willard S., Jr.: A Summary of the Low-Lift Drag and Longitudinal Trim Characteristics of Two Versions of an Interceptor-Type Airplane As Determined From Flight Tests of Rocket-Powered Models at Mach Numbers Between 0.75 and 1.78. NACA RM L54H31, 1954.
5. Silverstein, Abe, and White, James A.: Wind-Tunnel Interference With Particular Reference to Off-Center Positions of the Wing and to the Downwash at the Tail. NACA Rep. 547, 1936.
6. Gillis, Clarence L., Polhamus, Edward C., and Gray, Joseph L., Jr.: Charts for Determining Jet-Boundary Corrections for Complete Models in 7- by 10-Foot Closed Rectangular Wind Tunnels. NACA WR L-123, 1945. (Formerly NACA ARR L5G31.)
7. Jaquet, Byron M.: Calculated Lateral Frequency Response and Lateral Oscillatory Characteristics for Several High-Speed Airplanes in Various Flight Conditions. NACA RM L53J01, 1953.

TABLE I.- DIMENSIONS OF MODEL

Wing:	
Aspect ratio . . . . .	3.56
Span, ft . . . . .	3.018
Area, sq ft . . . . .	2.567
Mean aerodynamic chord, ft . . . . .	0.935
Taper ratio . . . . .	0.30
Sweep angle of quarter-chord line, deg . . . . .	45
NACA airfoil section parallel to plane of symmetry . . . . .	64(06)A007
Dihedral angle, deg . . . . .	0
Twist, deg . . . . .	0
Incidence, deg . . . . .	0
Ailerons:	
Inboard-end location, percent semispan . . . . .	32.3
Outboard-end location, percent semispan . . . . .	75.0
Chord, percent wing chord . . . . .	25
Spanwise gaps . . . . .	Sealed
Chordwise gaps . . . . .	Open
Horizontal Tail:	
Aspect ratio . . . . .	3.56
Span, ft . . . . .	1.548
Area, sq ft . . . . .	0.676
Mean aerodynamic chord, ft . . . . .	0.479
Taper ratio . . . . .	0.30
Sweep angle of quarter-chord line, deg . . . . .	45
NACA airfoil section parallel to plane of symmetry . . . . .	64A003.5
Dihedral angle, deg . . . . .	0
Twist, deg . . . . .	0
Incidence, deg . . . . .	0
Tail length from center of gravity to $\bar{c}/4$ of tail, ft . . . . .	1.148
Vertical Tail:	
Small:	
Aspect ratio . . . . .	1.28
Span from reference line, ft . . . . .	0.647
Area to reference line, sq ft . . . . .	0.328
Exposed area, sq ft . . . . .	0.249
Mean aerodynamic chord, ft . . . . .	0.542
Taper ratio . . . . .	0.369
Sweep angle of quarter-chord line, deg . . . . .	45
NACA airfoil section parallel to fuselage reference line . . . . .	64A003.5
Tail length from center of gravity to $\bar{c}/4$ of tail, ft . . . . .	1.163
Large:	
Aspect ratio . . . . .	1.58
Span from reference line, ft . . . . .	0.797
Area to reference line, sq ft . . . . .	0.403
Exposed area, sq ft . . . . .	0.317
Mean aerodynamic chord, ft . . . . .	0.561
Taper ratio . . . . .	0.270
Sweep angle of quarter-chord line, deg . . . . .	45
Airfoil section . . . . .	3.5 percent thick (modified flat plate)
Tail length from center of gravity to $\bar{c}/4$ of tail, ft . . . . .	1.203

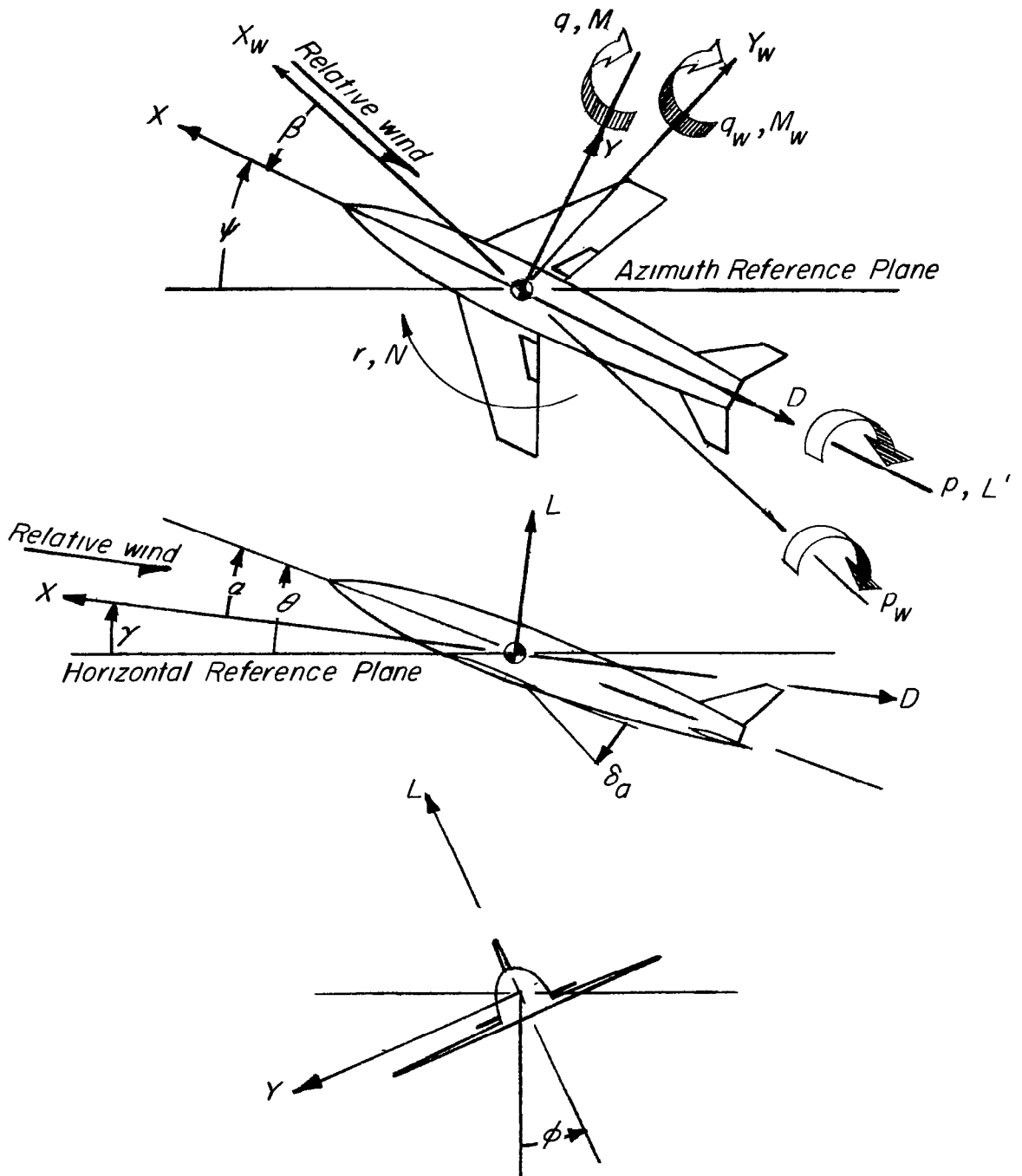


Figure 1.- Systems of stability and wind axes. Arrows indicate positive directions of forces, moments, and angular displacements. Symbols with subscript w indicate wind axes.

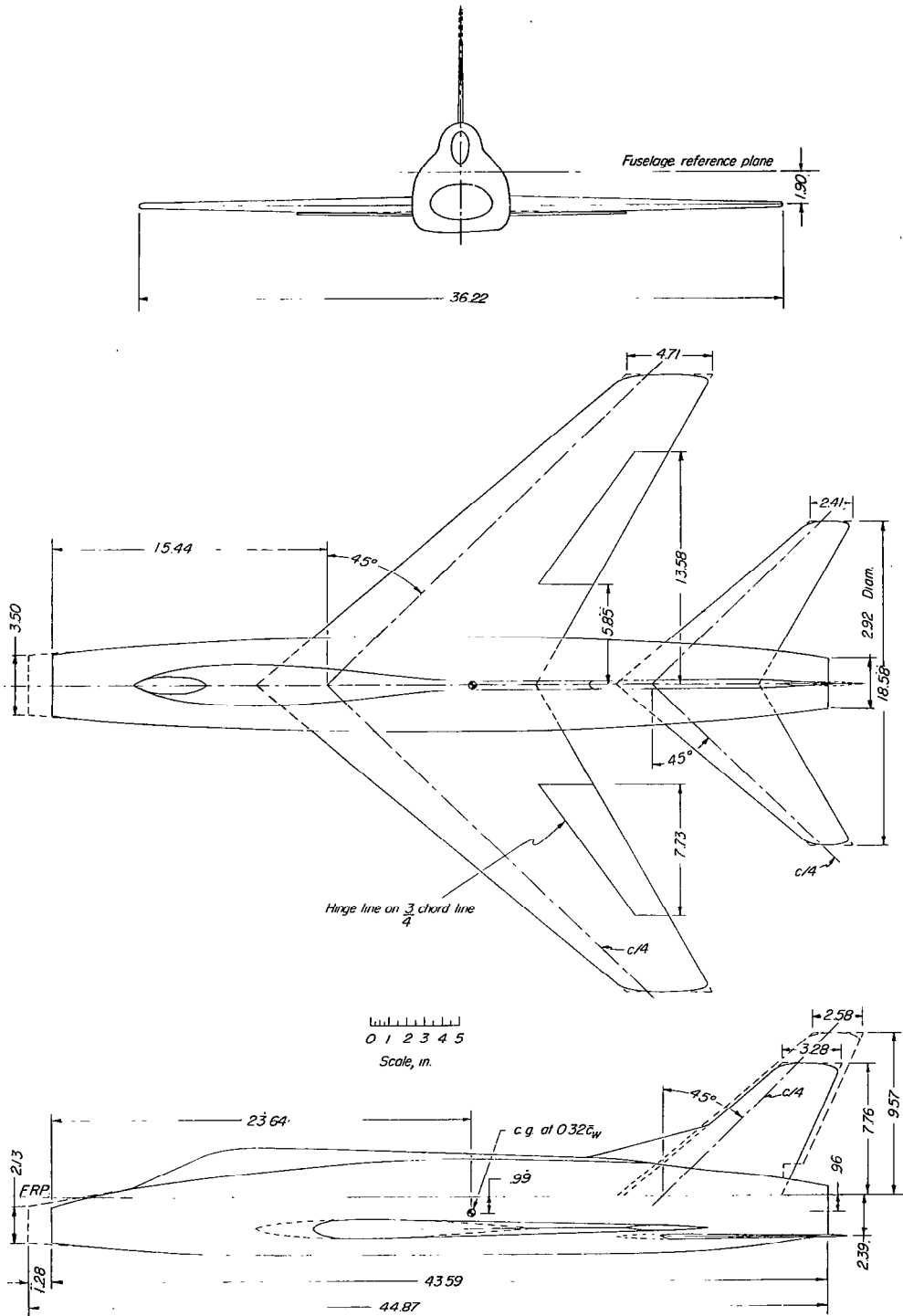


Figure 2.- Three-view drawing of 0.0825-scale model of a 45° swept-wing fighter-type airplane. All dimensions are in inches.

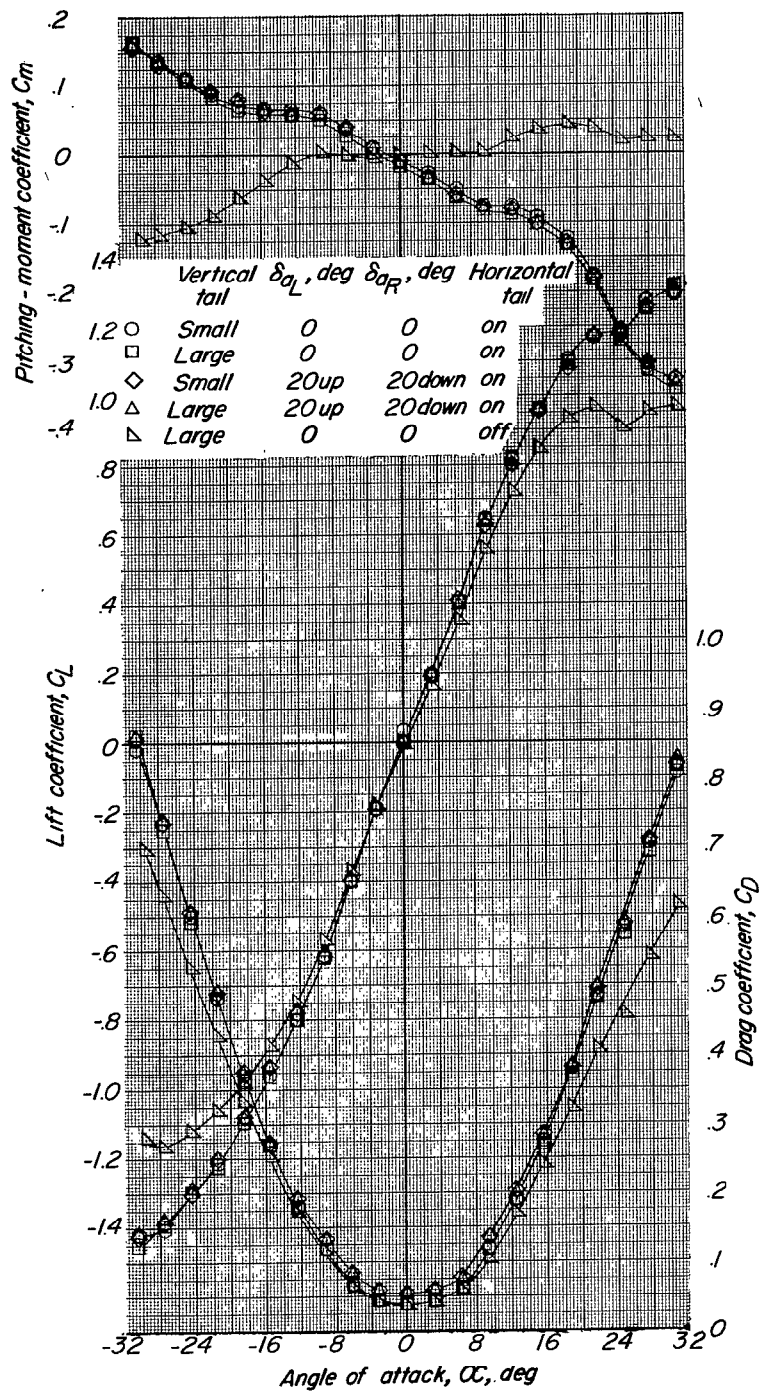
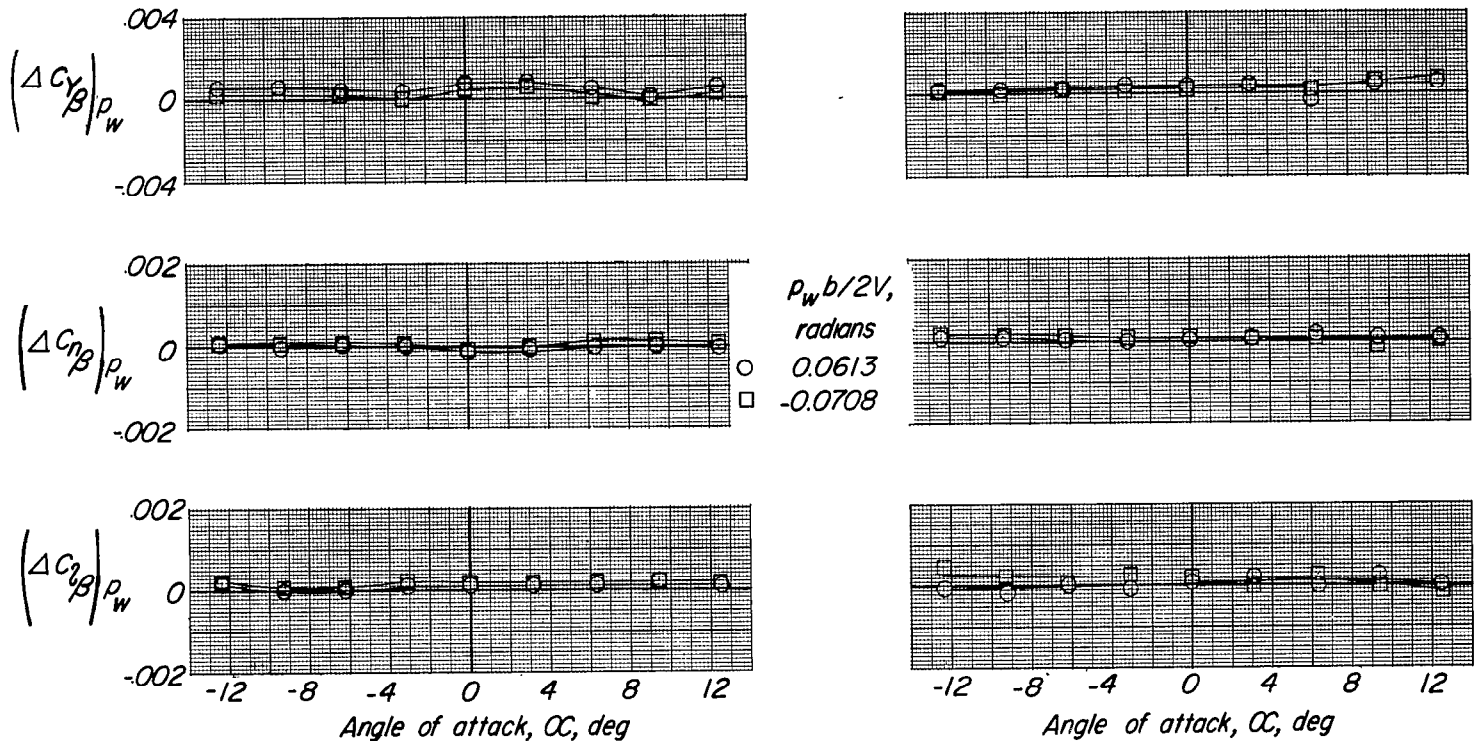


Figure 3.- Variation of  $C_m$ ,  $C_L$ , and  $C_D$  with  $\alpha$  for 0.0825-scale model of a  $45^\circ$  swept-wing airplane with extended-nose fuselage.  $\beta = 0^\circ$ ;

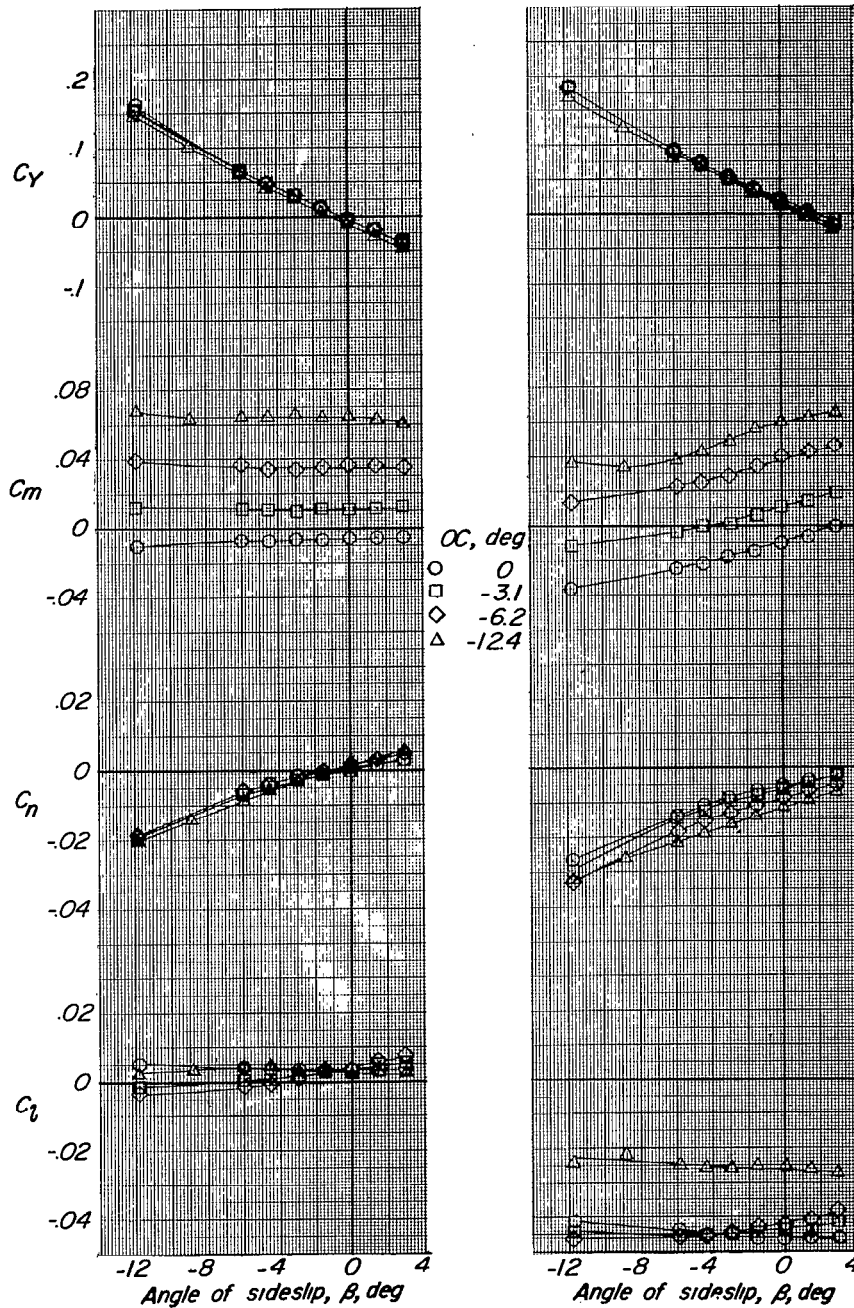
$$\frac{p_w b}{2V} = 0; \quad \frac{r b}{2V} = 0; \quad \frac{q \bar{c}}{2V} = 0.$$



(a)  $\delta_{aL} = 0^\circ$ ;  $\delta_{aR} = 0^\circ$ .

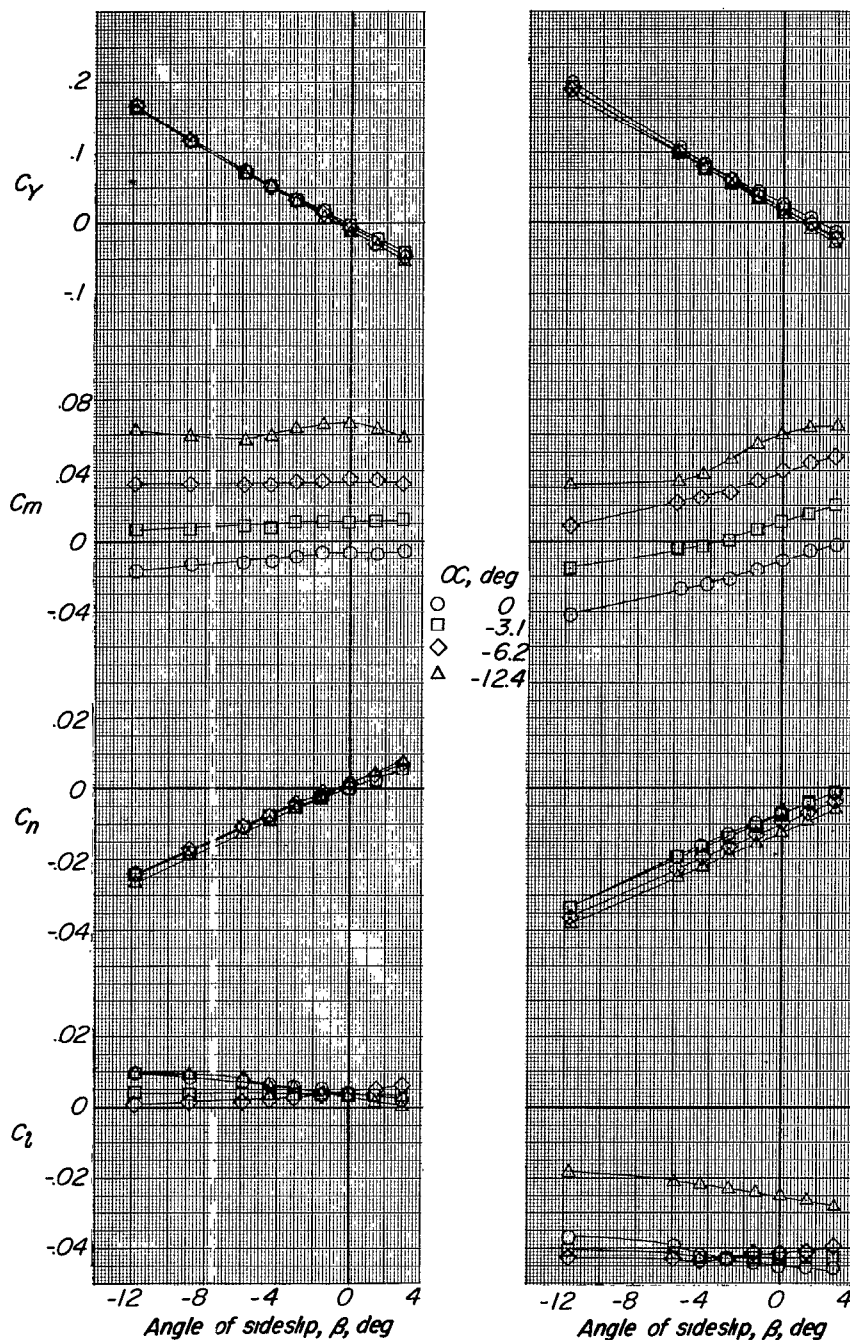
(b)  $\delta_{aL} = 20^\circ$  up;  $\delta_{aR} = 20^\circ$  down.

Figure 5.- Effect of  $\frac{p_w b}{2V}$  on static lateral stability derivatives of 0.0825-scale model of a  $45^\circ$  swept-wing airplane with extended-nose fuselage and small vertical tail.  $\beta = \pm 6^\circ$ .



(a)  $\delta_{aL} = 0^\circ$ ;  $\delta_{aR} = 0^\circ$ . (b)  $\delta_{aL} = 20^\circ$  up;  $\delta_{aR} = 20^\circ$  down.

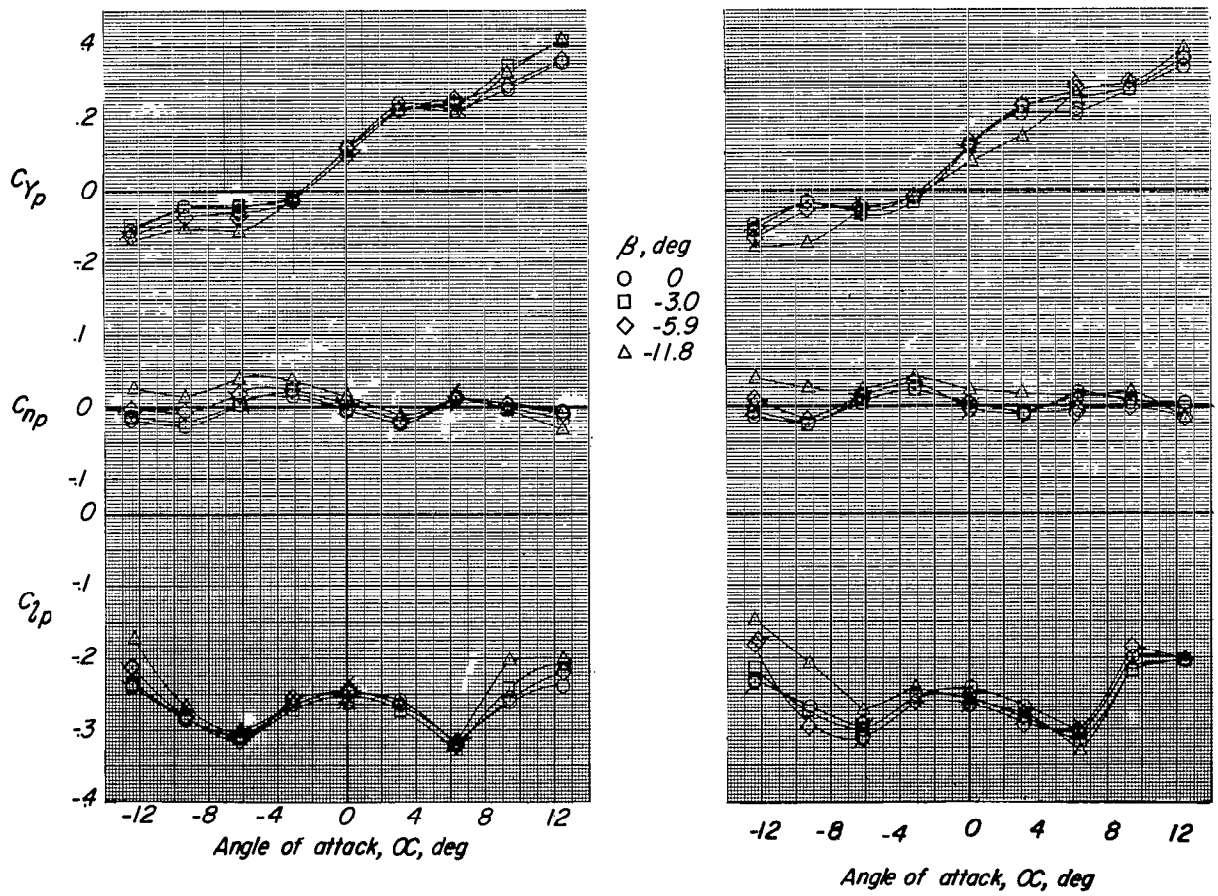
Figure 6.- Variation of  $C_Y$ ,  $C_M$ ,  $C_N$ , and  $C_L$  with  $\beta$  for several angles of attack for 0.0825-scale model of a  $45^\circ$  swept-wing airplane with extended-nose fuselage and small vertical tail.



(a)  $\delta_{aL} = 0^\circ$ ;  $\delta_{aR} = 0^\circ$ .

(b)  $\delta_{aL} = 20^\circ$  up;  $\delta_{aR} = 20^\circ$  down.

Figure 7.- Variation of  $C_Y$ ,  $C_m$ ,  $C_n$ , and  $C_l$  with  $\beta$  for several angles of attack for 0.0825-scale model of a  $45^\circ$  swept-wing airplane with extended-nose fuselage and large vertical tail.



(a)  $\delta_{aL} = 0^\circ$ ;  $\delta_{aR} = 0^\circ$ .

(b)  $\delta_{aL} = 20^\circ$  up;  $\delta_{aR} = 20^\circ$  down.

Figure 8.- Variation of  $C_{Yp}$ ,  $C_{np}$ , and  $C_{lp}$  with  $\alpha$  and  $\beta$  for 0.0825-scale model of a  $45^\circ$  swept-wing airplane with short-nose fuselage and small vertical tail. Flagged symbols are for extended-nose fuselage.

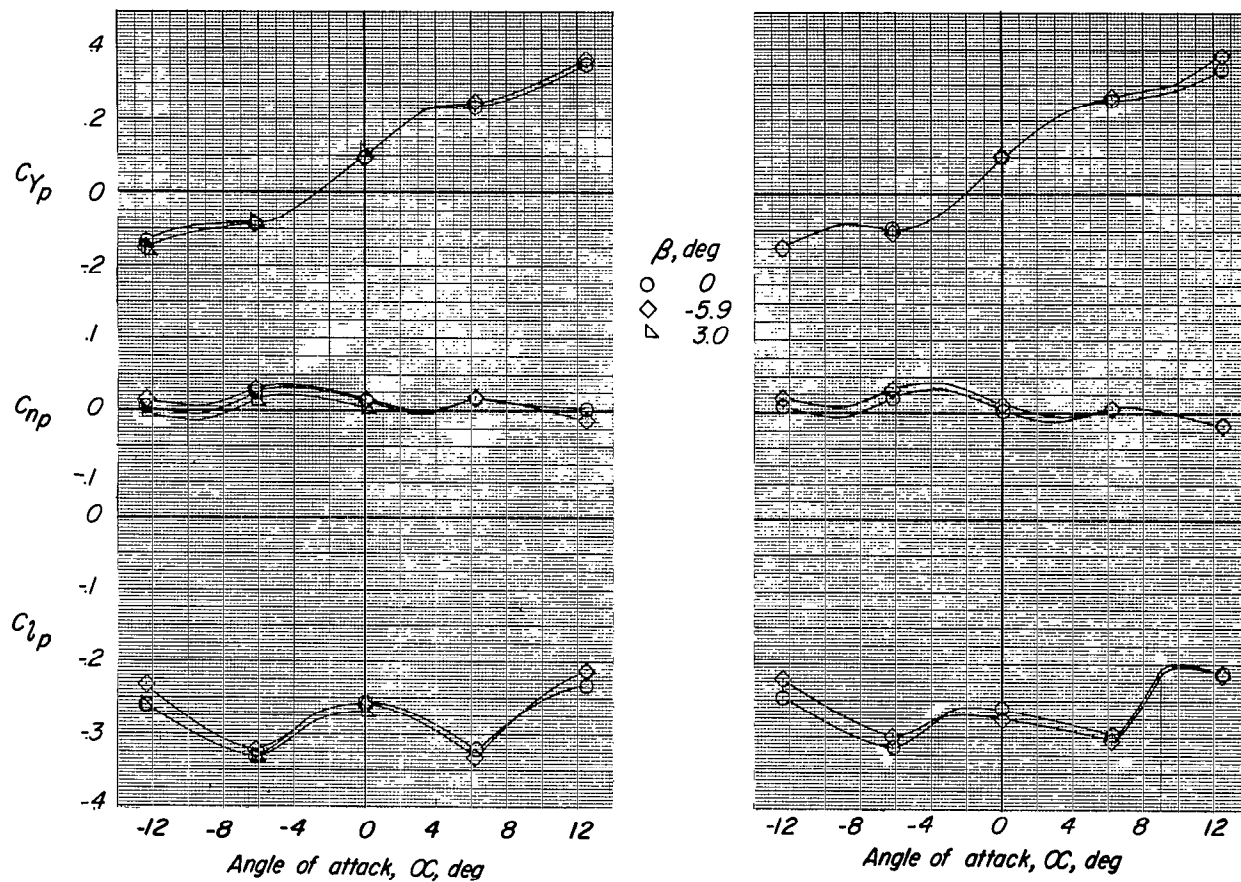
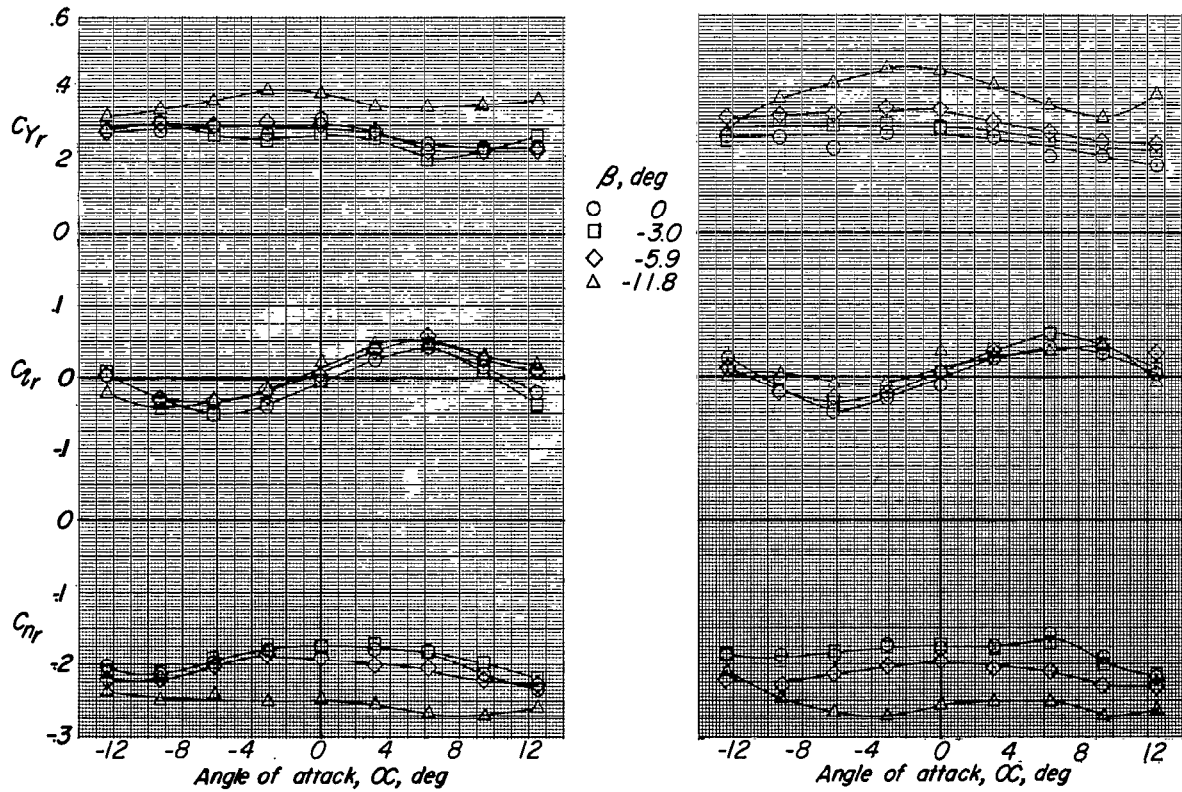
(a)  $\delta_{aL} = 0^\circ$ ;  $\delta_{aR} = 0^\circ$ .(b)  $\delta_{aL} = 20^\circ$  up;  $\delta_{aR} = 20^\circ$  down.

Figure 9.- Variation of  $C_{Y_p}$ ,  $C_{n_p}$ , and  $C_{l_p}$  with  $\alpha$  and  $\beta$  for 0.0825-scale model of a  $45^\circ$  swept-wing airplane with extended-nose fuselage and large vertical tail.



(a)  $\delta_{a_L} = 0^\circ$ ;  $\delta_{a_R} = 0^\circ$ .

(b)  $\delta_{a_L} = 20^\circ$  up;  $\delta_{a_R} = 20^\circ$  down.

Figure 10.- Variation of  $C_{Yr}$ ,  $C_{l_r}$ , and  $C_{n_r}$  with  $\alpha$  and  $\beta$  for 0.0825-scale model of a  $45^\circ$  swept-wing airplane with extended-nose fuselage and small vertical tail.

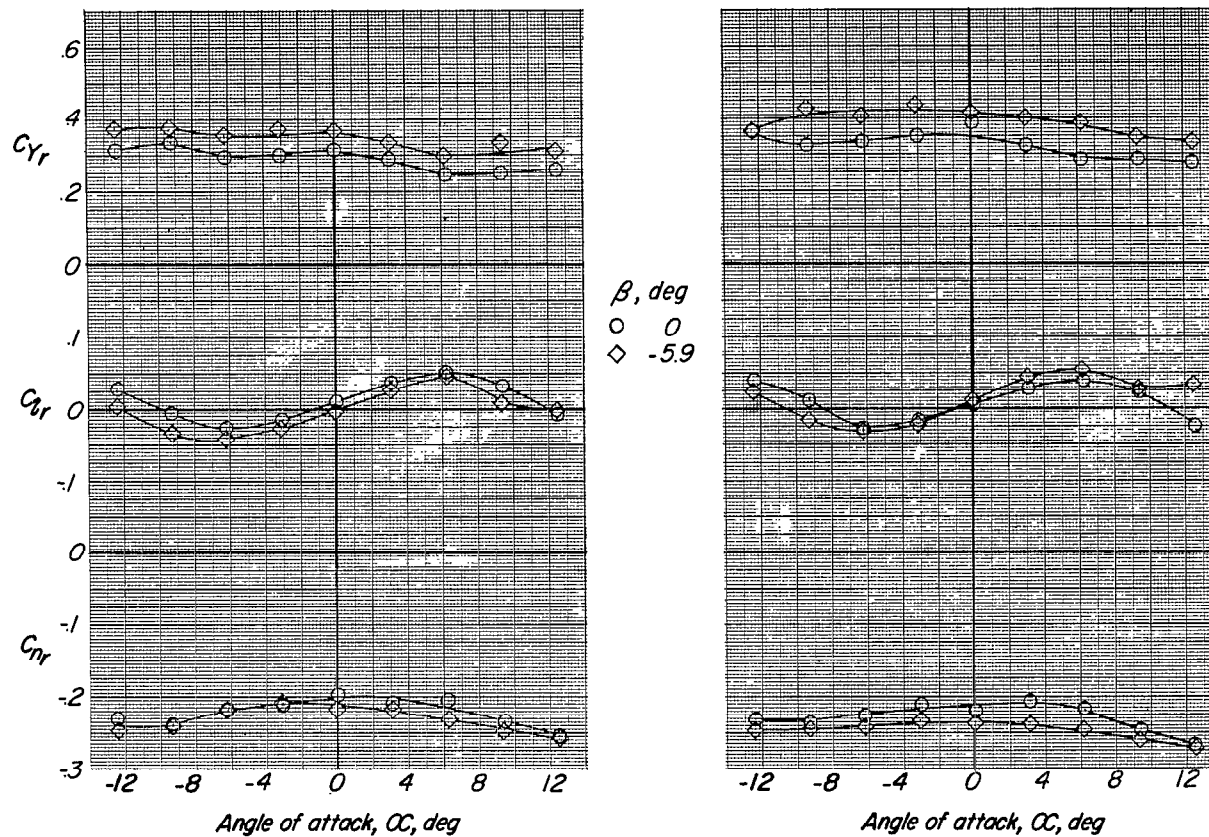
(a)  $\delta_{a_L} = 0^\circ$ ;  $\delta_{a_R} = 0^\circ$ .(b)  $\delta_{a_L} = 20^\circ$  up;  $\delta_{a_R} = 20^\circ$  down.

Figure 11.- Variation of  $C_{Y_r}$ ,  $C_{l_r}$ , and  $C_{n_r}$  with  $\alpha$  and  $\beta$  for 0.0825-scale model of a  $45^\circ$  swept-wing airplane with extended-nose fuselage and large vertical tail.

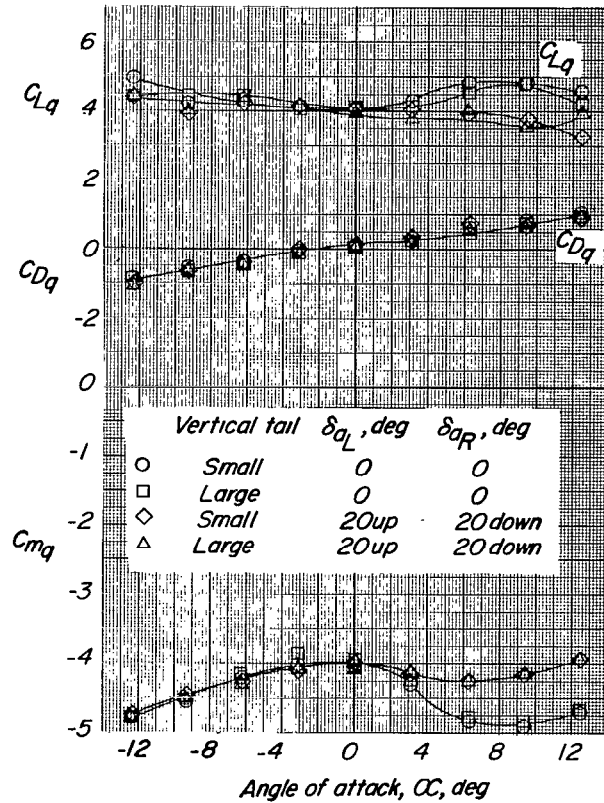


Figure 12.- Variation of  $C_{Lq}$ ,  $C_{Dq}$ , and  $C_{mq}$  with angle of attack for 0.0825-scale model of a  $45^\circ$  swept-wing airplane with extended-nose fuselage.  $\beta = 0^\circ$ .

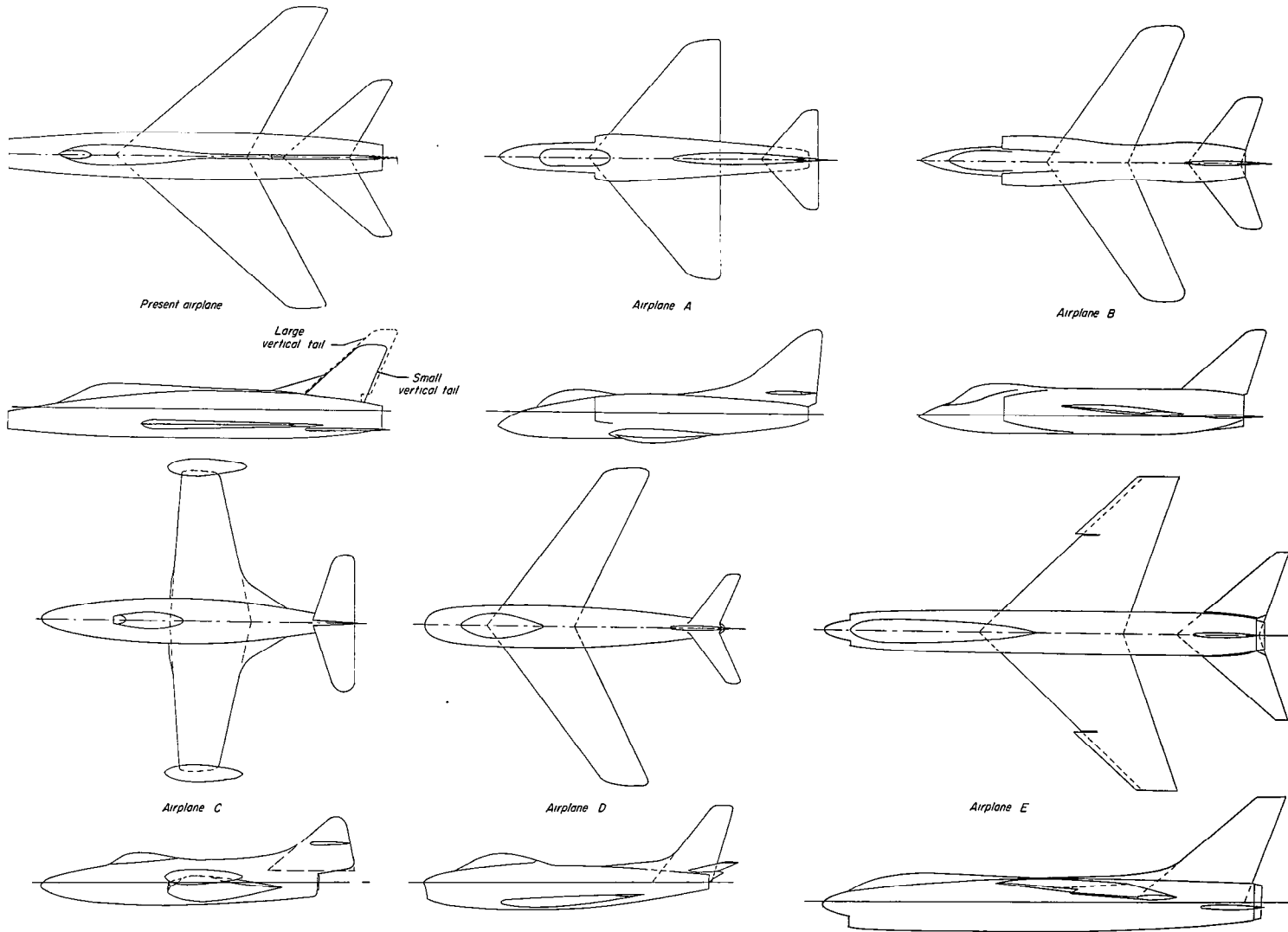


Figure 13.- Airplanes used in figure 14. All are drawn to approximately same scale.

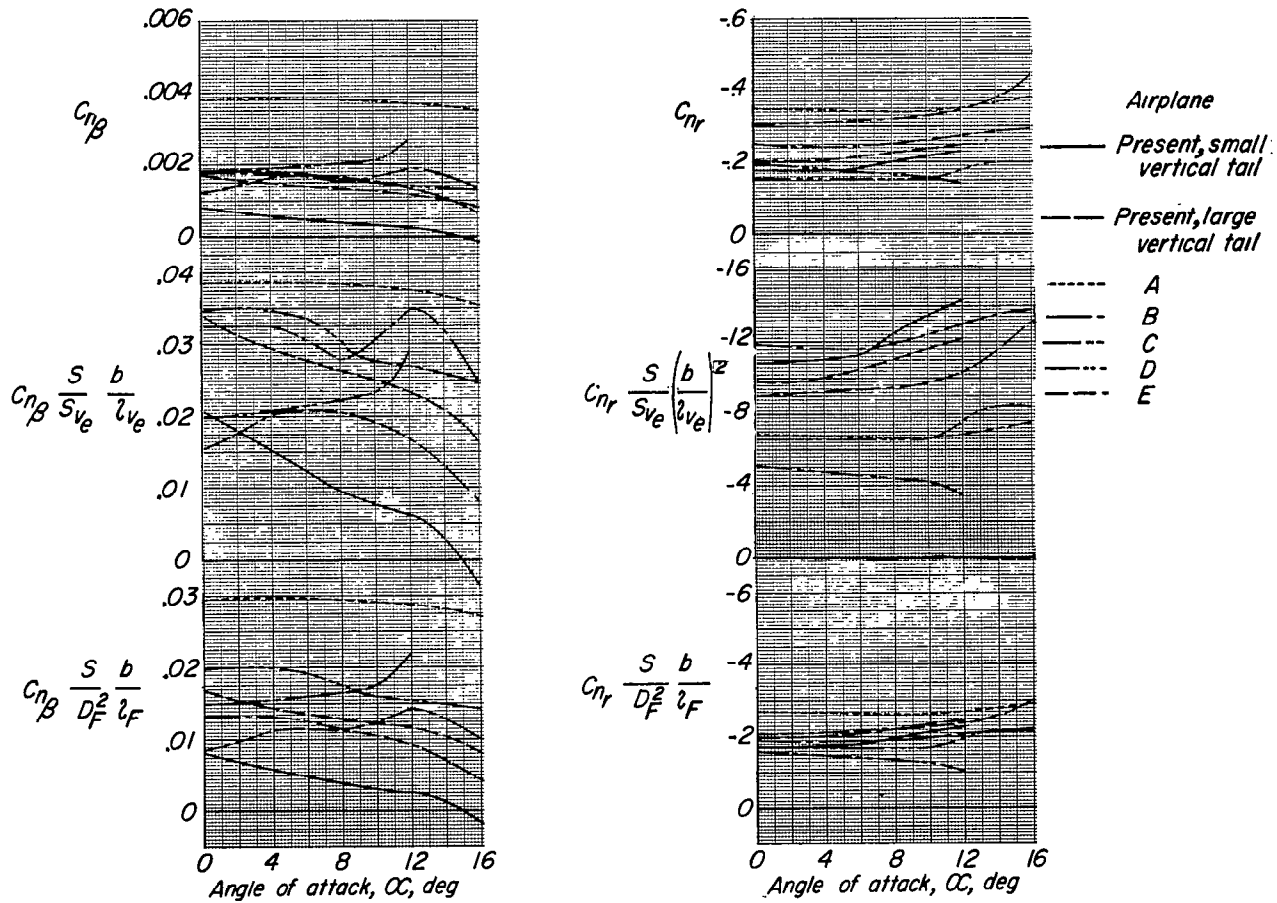


Figure 14.- Variation for several airplanes of the derivatives  $C_{n\beta}$  and  $C_{nr}$  with  $\alpha$ , when based on the wing, vertical-tail, and fuselage dimensions.

NASA Technical Library



3 1176 01438 0357

CONFIDENTIAL